symmetry

MDPI

Article

Hydrodynamic-Interaction Analysis of an Autonomous Underwater Hovering Vehicle and Ship with Wave Effects

Chen-Wei Chen, Ying Chen * and Qian-Wen Cai

Ocean College, Zhejiang University, Zhoushan 316000, China; cwchen@zju.edu.cn (C.-W.C.); 21634097@zju.edu.cn (Q.-W.C.)

* Correspondence: ychen@zju.edu.cn

Received: 17 August 2019; Accepted: 25 September 2019; Published: 29 September 2019

Abstract: A new vertical axis-symmetrical dish-shaped autonomous underwater vehicle (AUV) with excellent maneuverability, known as the autonomous underwater hovering vehicle (AUH), is proposed. This study investigates an important working model of the AUH approaching a host ship in waves. The working model of AUH–Ship interactions deals with hydrodynamic interaction, seakeeping performance for communication, launch, and recovery near a free surface. The AUH is able to navigate and implement homing automation through acoustic positioning equipment, a depth sensor, a heading compass, and a Doppler velocity log (DVL) in the working area based on numerical analysis of AUH–Ship hydrodynamic performance in this study. The hydrodynamic-interaction performance of the AUH and ship near free surfaces is analyzed in the frequency and time domains using a potential-based surface-panel method based on a commercial computational fluid dynamics (CFD) solver (ANSYS-AQWA), i.e., a 3D panel code of seakeeping performance module in the ANSYS platform where the fluid is assumed to be irrotational, inviscid, and incompressible. The motion performance of the AUH approaching the host ship, with a dynamic positioning system in waves, is studied by estimating interactive response-amplitude operators (RAOs) of the AUH and host ship in 6-DOF that were estimated and analyzed at different wave amplitudes and frequencies. In the ship and AUH interaction simulations, the host ship is assumed to be a well-posed station keeping in waves with zero service speed. The AUH and ship interference effect is studied at different distances to appropriate recovery and launch positions for the AUH at the following sea and beam sea, i.e., wave-encounter angles 0° and 90°, respectively. In addition, the hydrodynamic interaction of the AUH and ship in yaw and roll at different AUH velocities is estimated. The AUH motion performance approaching the ship in long-crested irregular seas is analyzed in the time domain using the Pierson–Moskowitz wave spectrum model. Viscid hydrodynamic force on AUH motion in roll near a free surface was significant. A damping model was adopted to formulate the viscid effect to enhance the effectiveness of the ANSYS-AQWA inviscid potential-based solver. Numerical analysis of motion RAO of the AUH in roll with the damping effect was compared to the experimental data in wave-frequency range 0.2–1.0 Hz, resulting in the average error being reduced from 21.03% to 9.95% to verify the method's accuracy. The proposed method conveniently and accurately predicted hydrodynamic-interaction characteristics and motion RAO for a dish-type AUH and host ship for the precise use of mounted sensors in waves. The results of these simulations can be used to analyze the homing automation and adaptive controllability to advance the AUV development and design.

Keywords: Autonomous Underwater Vehicle (AUV); Autonomous Underwater Hovering Vehicle (AUH); hydrodynamic interaction; response amplitude operator (RAO); wave effects

1. Introduction

From oceanographic investigations to military applications, new axisymmetric types of autonomous underwater vehicles (AUVs) have been developed to conduct missions in complex marine environments in recent years [1,2]. The highly autonomous, flexible, maneuverable, and controllable overall design of AUVs plays an important role in ocean exploration and development.

Development of a launch-and-recovery system for AUVs from a research vessel is significant to the overall design. Submarine analysis of launch-and-recovery underwater-vehicle models was carried out by Chen and Su in 2011 [3]. An automated launch-and-recovery system for AUVs from an unmanned surface vehicle was proposed by Sarda and Dhanak in 2017 [4]. However, hydrodynamic-interaction effects of wave-induced disturbance on the surface vehicle and axisymmetric AUVs were ignored in these studies.

Research on the hydrodynamic-interaction performance of wave-induced disturbance on a hovering AUV and a host ship is significant to the overall design process of the AUV and/or scientific-research ships to smoothly guarantee the successful deployment, operation, and homing automation of AUVs from the deep sea to the free surface, or launching from host ships into waves. However, quickly estimating wave-induced hydrodynamic-interaction forces between a vertical axisymmetric AUV hull form and large-scale host ship is difficult and challenging. The viscous computational fluid dynamic solver is a time-consuming method to solve a wave-induced and multibody hydrodynamic-interaction problem. Thus, an inviscid-potential-based surface-panel method is an efficient and effective method for solving fluid and rigid-body interaction problems. The potential flow modelling in the surface-panel method was assumed to be irrotational, inviscid, and incompressible.

Hydrodynamic-interaction performance of AUVs in waves is critical to attitude-controller design and has recently been receiving intensive attention. A few works have been done on the prediction of hydrodynamic-interaction forces and moments between surface and underwater vessels [5–8]. The hydrodynamic-interaction issues associated with AUVs approaching a cone-shaped dock in ocean currents were studied in the literature [5]. Xie et al. [6] presented an experimental study of wave loads on a small vehicle in close proximity to a large vessel. The results of this investigation could be adopted to inform planning marine operations, such as the recovery of an AUV from a mothership in low-to-moderate sea states.

Skomal et al. [7] presented a depth-limited AUV mounted with a viable tool for directly observing the behavior of marine animals in order to investigate the behavior, habitat, and feeding ecology of white sharks *Carcharodon carcharias* near Guadalupe Island, off the coast of Mexico. However, the hydrodynamic interactions between the AUV and waves were not considered in this study. In fact, the effect of hydrodynamic interaction on wave loads on the AUV model was substantial enough to cause inefficiently controlled vessel motions during such operations. Zhi et al. [8] presented quasistatic analysis of hydrodynamic interactions between an AUV and a host submarine for controlling the AUV recovered to the submarine well.

In the literature of seakeeping analysis of surface vessels or underwater vehicles, Tian et al. [9] presented research on the influence of surface waves on the hydrodynamic performance of an axis-symmetrical slender-body AUV when the AUV sailed near the free surface. The results showed that the variation of AUV hydrodynamic forces was significantly affected by the waves. Mansoorzadeh and Javanmard [10] adopted a two-phase flow CFD solver with the Volume of Fluid (VOF) model to investigate the free-surface effects on drag-and-lift coefficients of an AUV with an axisymmetric hull form. Much CPU time is needed when adopting this method. Therefore, Malik et al. [11] adopted the 3D panel method using the commercial CFD code, ANSYS-AWQA, to carry out the time-saving simulations of wave-force prediction on a slender underwater vehicle in the frequency and time domains.

Lighthill [12] studied second-order wave radiation and diffraction problems by using the 3D frequency-domain method, and proposed that second-order wave force can be obtained from virtual

radiation potential. Chen and Fang [13] analyzed the hydrodynamic interaction between two vessels traveling in close parallel waves. Choi and Hong [14], Masashi et al. [15], and Hong et al. [16] adopted the high-order boundary-element method in the frequency domain to evaluate hydrodynamic disturbance between multiple buoys. Their numerical simulation results were verified by physical-model tests. The literature review reveals that researchers have investigated hydrodynamic disturbances between large floating bodies, but few have focused on hydrodynamic disturbances between floating bodies with large size differences (e.g., an AUV and a host ship).

This study is focused on the prediction of the hydrodynamic performance of wave-induced disturbances on an AUV and a host ship for solving problems of motion and control of launching and recovery of AUVs from host ships in advance. A new dish-shaped AUV with a vertical axisymmetric hull form, the autonomous underwater hovering vehicle (AUH), is proposed and was developed by the Ocean College of Zhejiang University (ZJU) in 2016. The AUH was designed with a flying-saucer shape for enhanced maneuverability, to be efficient and effective and able to perform full circumferential steering, fixed-point hovering, and free take-off and landing on the sea bed. The designed speed of the AUH was 1 knot in surge. In low design speed, the horizontal maneuverability and vertical-motion stability of the disk-shaped AUH would be better than conventional torpedo-shaped AUVs [17]. Preliminary related research on the configurational design and system integration of the AUH prototype was implemented, including structural design with streamline-hull form, hybrid propulsion system with a buoyancy engine and four vectoring electric propellers, controller design in calm seas [18], analysis of seakeeping performance of second-order wave forces on the AUH [19], and prediction of antisea-current ability [20], and of added mass for the AUH near the sea bottom [21].

In addition, the AUH has motion-control, power-transmission, and optical-communication systems for the presentation of special homing automation functions in deep-sea and near-free-surface work. Excellent autonomous automation homing-navigation models have been published in the literature [22–25]. Miller et al. [22] proposed a navigation system integrating high-rate inertial-measurement-unit (IMU) accelerometers and gyros in allowable time propagation while multisensors provide measurement corrections. Bo et al. [23] proposed a SEIF-SLAM navigation approach to improve the accuracy and navigation of a slender AUV. Recently, a vision-based underwater-vehicle navigation system was proposed in the literature [24,25]. These vision-based navigation approaches could improve conventional acoustic-navigation approaches to enhance the efficiency and effectiveness of AUV recovery in clean sea water. Part of the mentioned navigation system was adopted and successfully extended by the AUH design in our navigation model. The overview of the AUH structure and module system encapsulated in the pressure hull is shown in Figure 1a,b, respectively. The ZJU AUH prototype is shown in Figure 1, and its main parameters (hull form, hybrid propulsion, and multidisciplinary systems) are shown in Table 1.

For AUH–Ship working conditions, hydrodynamic analysis should be done to understand AUH behavior in hydrodynamic interactions, allowing the advanced implementation of control strategies. Additionally, behavioral predictions for emerging and recovering an AUH from a ship in waves are important to advance AUH adaptive controllability, homing automation, and overall design.

Hydrodynamic modeling of AUH–Ship interactions near or on a free surface is challenging [26,27]. Intrinsically, waves are irregular, unsteady, nonuniform fluids with frequent breaking and vertexing effects. Hydrodynamic-wave forces can, theoretically, be divided into discrete forces: First-order wave-induced, low-varying disturbance (second-order wave excitation, wave mean drift, current, and wind forces), radiation, viscosity, etc.

Due to the significant size difference between AUH and scientific research ship (host ship), the AUH moving toward or away from the host ship is disturbed by distinct, ship-induced wave interference. If an appropriate hydrodynamic-interaction theory model is used to predict AUH–Ship motion performance, appropriate seakeeping locations can be determined for the AUH communicating with a nearby host ship mounted with active sonar.

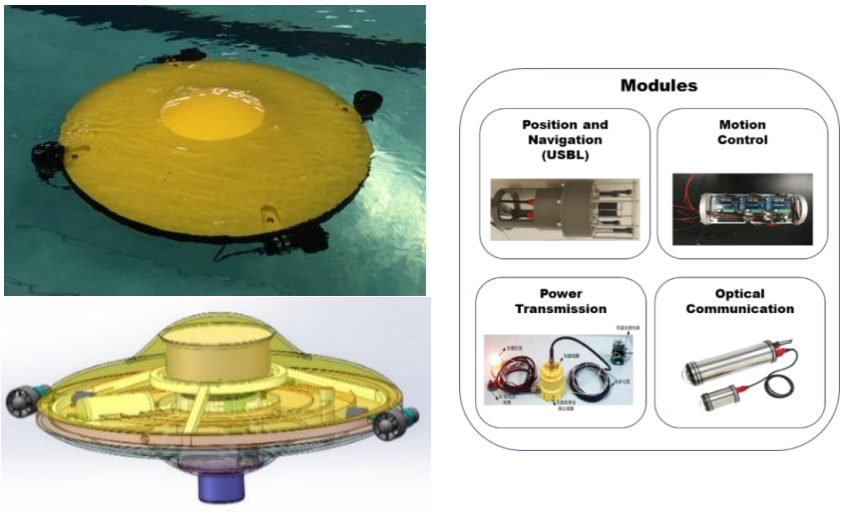

(**a**) (**b**)

Figure 1. Zhejiang University (ZJU) autonomous underwater hovering vehicle (AUH) prototype: (**a**) Structural design; (**b**) module system.

Table 1. Main parameters of Zhejiang University (ZJU) autonomous underwater hovering vehicle (AUH).

Parameter	Symbol	Unit	Value
Diameter	L	m	1.0
Height	T	m	0.44
Design depth	H	m	1000
Seawater density	ρ	$kg \cdot m^{-3}$	1020–1030
Design speed	U	$m \cdot s^{-1}$	0.5144–1.5432
Mass/payload	m	kg	122.6/15
Vertical distance between CG and CB	BG	mm	37
Battery	null	kwh/kg	2 * 12 V–30 Ah
Number of thrusters/thrust	null	kg	2/50 kgf
Buoyancy engines/volume	null	ml	2/500
USBL/DVL	null	null	AT: 50, 150 mm/20 kHz
Pressure hull	null	null	1

Seakeeping analysis of AUH–Ship interactions can improve AUH launch and recovery efficiency, staff safety at work, and can be conducted by studying the AUH–Ship Response Amplitude Operator (RAO). The RAO is used to study six-degrees-of-freedom (6-DOF) motion performance of marine vehicles maneuvering in waves that can be divided into two types: Motion RAO, i.e., the ratio of vehicle-motion amplitude to the amplitude of incident regular waves in the frequency domain (motion RAO utilizing the frequency-domain approach to evaluate radiation forces); and the force RAO, combined with the wave spectrum (obtaining loads for the sea state and sailing conditions) [19].

In the overall design of the AUH, a hydrodynamic-interaction study of the AUH–Ship relationship could significantly enhance the effectiveness and efficiency of launch and recovery operations from a vessel onto a free surface. This study thus focused on researching the hydrodynamic-interaction performance of the AUH and host ship. Considering computing efficiency, this study adopted a potential-based panel method based on an inviscid CFD solver, namely, ANSYS-AQWA software. In the seakeeping characteristics of the AQWA module, the hydrodynamic-interaction performance (wave radiation force and diffraction force) between two buoys can be efficient in calculations, and the system can be effectively integrated with a comprehensive consideration of random environmental loads: Wind, current, wave, surge load, and propulsion effect.

In this study, this ANSYS-AQWA panel method was used to study the hydrodynamic interactions between AUH and host ship considering the effect of random wave loads for the purpose of optimizing AUV positions for communication with, and recovery and launch from, a surface vessel in regular and long-crested irregular seas. Two aspects of AUH–Ship interaction were studied: Motion RAO variations in AUH–Ship interactions with 6-DOF, and AUH–Ship interaction motions in irregular waves. The relationship between AUH and ship distances, and hydrodynamic disturbances was analyzed to determine suitable positions for launch and recovery. Cases studies were conducted evaluating different near-ship AUH locations, motion RAOs in 6-DOF, and AUH motion performance in the time domain. In addition, viscous hydrodynamic forces on the vertical axis-symmetrical AUH motion in roll or pitch near a free surface is significant. A damping model was adopted to formulate viscous effect to enhance effectiveness of the ANSYS-AQWA inviscid potential-based CFD solver. Numerical analysis of motion RAO of the AUH in roll with the damping effect were compared to experimental data in the range of wave frequency 0.2–1.0 Hz, resulting in average errors reduced from 21.03% to 9.95% to verify the method accuracy.

In the following sections, a mathematical model of a surface-panel method describing rigid-body hydrodynamic interactions in potential flow with wave effects is presented. In Section 3, simulation results of hydrodynamic interactions of AUH and host ship are introduced. The AUH and ship interference effect was studied at different distances for appropriate recovery and launch positions for the AUH at following, beam, and irregular seas. The motion RAO of the AUH near the ship in waves was estimated to determine the optimal positions to recover the AUH. In Section 4, the experiments of AUH motion RAO in rolling degrees of freedom are presented. The experiments were implemented in the large-scale cross-sectional wave flume of Zhejiang University Ocean College in Zhoushan in December 2017. Finally, the concluding remarks are presented in Section 5.

2. Mathematical Model

Modeling multibody hydrodynamic interference using a potential surface-panel method is presented and the definition of the coordinate system and the wave-encounter angle are presented in this section.

2.1. Coordinate System and Wave-Encounter Angle

The AUH–Ship interaction simulations contained a free surface, host ship, and AUH in the coordinate system, as shown in Figure 2a. Coordinate system O-XYZ is an inertial coordinate system. Coordinate systems O_1-$X_1Y_1Z_1$ and O_2-$X_2Y_2Z_2$ are the body-fixed coordinate systems of the host ship and the AUH, respectively (translating-rotation coordinates). Their hulls oscillated with the body-fixed coordinate systems. All coordinate-system origins were located on the hydrostatic surface using the right-hand coordinate system. Origin point O_1 was located at the center of gravity of the host ship, the positive OX_1 axis coincided with the navigation direction of the ship, and the OZ_1 axis was vertical (positive in the upward direction).

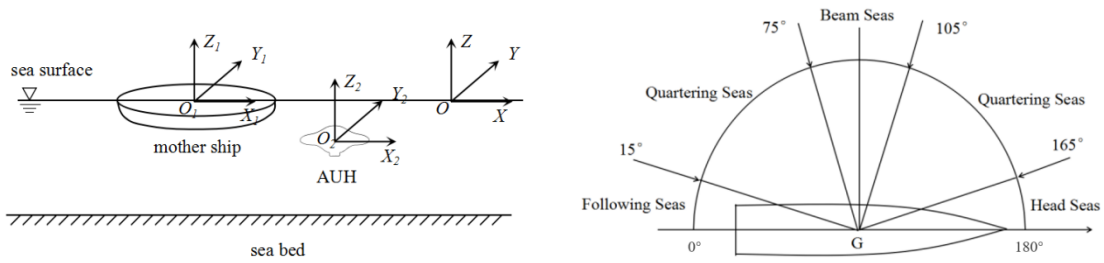

(**a**) (**b**)

Figure 2. (**a**) Definition of coordinate system between the AUH and host ship; (**b**) wave-encounter angle.

When the host ship and AUH navigated in waves, they were subject to wave impact from all directions. These wave angles could be divided into four categories [28]: Following sea, quartering sea, beam wave, and head sea. The host ship and AUH both had 6-DOF motion in the waves, as shown in Figure 2b.

2.2. Potential Surface-Panel Method

Fluid was assumed to be irrotational, inviscid, and incompressible based on potential-flow theory. The floating-body system in the computational domain behaved as a simple harmonic with slight wave motion. The following velocity-potential function satisfied the Laplace equation [29]:

$$\nabla^2\Phi = 0 \tag{1}$$

where Φ is the velocity potential

$$\Phi = -Ux + \phi \tag{2}$$

in which the term $-Ux$ denotes AUH sailing at constant speed U, and ϕ denotes perturbation potential induced by the presence of the AUH.

Two floating bodies were present near the flow field, making the total velocity of the flow field [30]

$$\Phi(x,y,z,t) = \Phi_I(x,y,z,t) + \Phi_D(x,y,z,t) + \Phi_R^1(x,y,z,t) + \Phi_R^2(x,y,z,t) \tag{3}$$

where Φ_I represents the velocity potential of the incident wave, Φ_D represents the diffraction power of multifloating system, Φ_R^1 represents the radiation potential of Floating Body 1 in the multifloating system, and Φ_R^2 represents the radiation potential of Floating Body 2 in the multifloating system.

The steady-state response of Φ_D can be expressed as

$$\Phi_D(x,y,z,t) = \mathrm{Re}\left\{\phi_D(x,y,z)e^{-iwt}\right\} \tag{4}$$

where Re{} represents the real portion of the amount in {} and ω represents the wave frequency.

The radiation potential of the floating body m in a floating body system is

$$\Phi_R^{(m)}(x,y,z,t) = \mathrm{Re}\left\{\phi_R^{(m)}(x,y,z)e^{-iwt}\right\} \tag{5}$$

where $\phi_R^m = i\omega \sum_{j=1,6} \xi_j\phi_j$, ξ_j denotes the 6-DOF motion amplitudes and m denotes multi-marine buoys.

The Laplace equation and free surface, object surfaces, bottom, and far-field radiation conditions for each of these buoys should be satisfied by these value calculations constrained by boundary conditions. These boundary conditions, including free surface, sea bed, body boundary, radiation, and initial conditions were considered. The Laplace equation and free surface, object surface, bottom, and far-field radiation conditions for each of these buoys should be satisfied as following:

1. Body Boundary Condition

The Neumann condition was obtained based on a zero-flux condition for fluid across the boundary:

$$\left.\frac{\partial\phi}{\partial n}\right|_{S_B} = \mathbf{U}\cdot\mathbf{n} \tag{6}$$

where $\mathbf{U}\cdot\mathbf{n}$ denotes normal velocity on AUH boundary S_B due to its motion.

2. Sea Bottom Boundary Condition

The zero-flux condition for fluid across the sea-bottom boundary was calculated as

$$\left.\frac{\partial\phi}{\partial n}\right|_{S_H} = 0 \tag{7}$$

where S_H denotes the sea-bottom boundary.

3. Combined Kinematic and Dynamic Free Surface Conditions

$$\left[\left(i\omega_e - U\frac{\partial}{\partial x}\right)^2 + g\frac{\partial}{\partial z}\right]\phi = 0 \text{ on z} = 0 \tag{8}$$

where ω_e denotes encounter frequency, z denotes depth in sea.

4. Boundary Condition at Infinity

The disturbance generated by the AUH body vanished as distance r approached infinity:

$$\nabla\phi \to 0 \text{ as } r \to \infty \tag{9}$$

In concluding remarks, the problem-saving process can be illustrated: To solving the Laplace equation constrained by the above boundary conditions, we can get the velocity potential. Taking gradient of the velocity potential, the velocity distribution on the surfaces of the AUH and host ship can be obtained. Then, the AUH–Ship–Wave hydrodynamic interaction loads on the AUH can be obtained by adopting well-known Bernoulli equation of motion.

3. Simulation Results

In this section, numerical analysis that was carried out of AUH–Ship–Wave interactions is outlined. These case studies include: (1) AUH and host ship traveling at 0 knot speed in regular waves; (2) AUH traveling at 0.5–3.0 knot speed approaching the host ship; (3) AUH and host ship interacting in irregular waves with significant wave height (1 m), the Pierson–Moskowitz(P–M) wave-spectrum model adopted. In these cases, it is assumed that the mother ship has zero speed due to executing the dynamic positioning system which enables the ship to be fixed on the homing location of the AUH in waves. The initial set and layout of these simulations are shown in Figure 3.

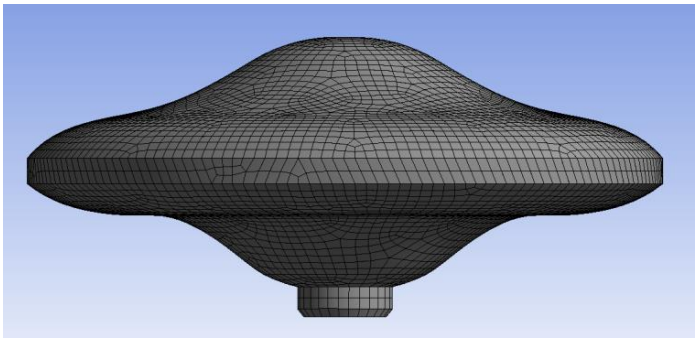

(**a**)

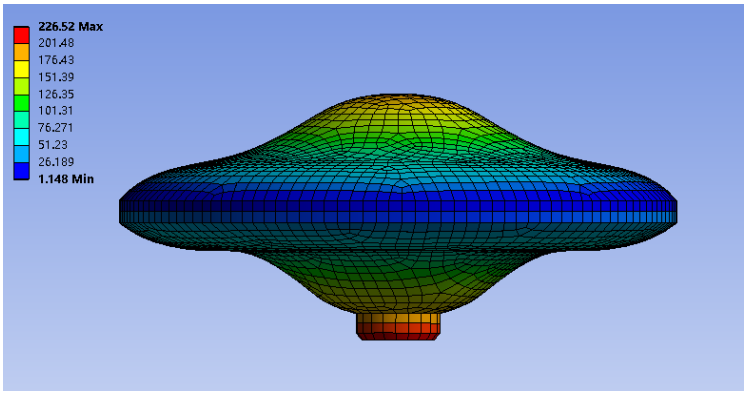

(**b**)

Figure 3. *Cont.*

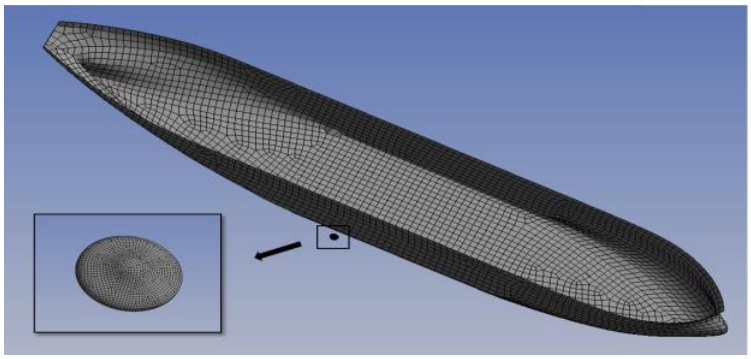

(**c**)

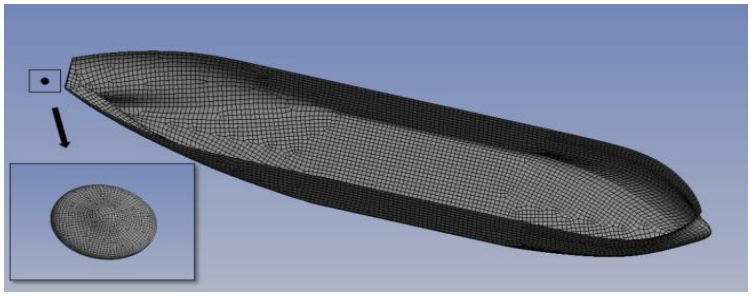

(**d**)

Figure 3. (**a**) Grids on the AUH surface with numbers of 6219 panels; (**b**) pressure distribution on the AUH panel surface with wave frequency of 1.48 rad/s; (**c**) the AUH approaching the midship of the host ship; (**d**) the AUH approaching the stern of the host ship.

3.1. Variations of Motion RAOs in AUH–Ship Interactions

The study calculated the 6-DOF RAOs [31,32] for AUHs located in three different positions along the X_1-axis of the host ship. RAOs are a concept in engineering statistics used to describe the motion responses of a floating buoy moving in the field of a ship or buoy design. This is performed by a transfer function that transforms wave excitation to floating-body movement while incorporating the effects of diffraction and radiation. Motion RAOs in 6-DOF motions for different sailing conditions can be expressed as

$$RAO(\omega_E, \chi) = \eta_i(\omega_E, \chi)/\zeta(\omega_E, \chi), \tag{10}$$

where η_i represents the magnitude of the i-DOF of the floating body, ζ represents the amplitude of a certain wave height in random wave conditions, ω_E represents encounter frequency, and χ represents encounter angle. When the amplitude is constant, larger RAO values correspond with greater floating-body-movement amplitudes in the i-DOF. Additionally, force RAOs can be directly derived using these determined motion RAOs as a base.

The degree of interference the host ship exerts on the AUH changes with the distance between the two. Identifying the position where the host ship influences the AUH could improve the feasibility and safety of AUH recovery, saving related resources. This study used the following parameters: Ship length L = 20 m, beam B = 4 m, draft t = 0.85 m, and AUH sizes shown in Tables 2 and 3 for three case studies (AUHs located at different host-ship X_1-coordinates). The host ship and AUH were both simulated to be travelling at speeds of 0 knots. The degree of interference the host ship exerted upon the AUH was investigated when the two floating bodies were at different distances in following sea (wave direction was 0°). The AUH was located in the three different X_1-axis positions shown in Table 2.

Table 2. Case study of AUH located in different X_1 coordinates.

Position	X_1 (m)	Y_1 (m)	Z_1 (m)
1	10	−2.4	−2
2	7	−2.4	−2
3	3	−2.4	−2

Table 3. Case study of AUH located in different Y_1 coordinates.

Position	X_1 (m)	Y_1 (m)	Z_1 (m)
1	10	−2.4	−2
2	10	−5	−2
3	10	−10	−2

The 6-DOF RAOs of the AUH were calculated for this study as shown in Figure 4a–d, where the AUH experienced disturbances (interference) from the host ship. Four degrees of freedom (surge, heave, roll, and pitch) were selected for the AUH–Ship interaction case studies, and the three curves shown for each of these represent the RAO variations versus wave frequencies in the three X_1-axis positions. $X_1 - Y_1$ plane positioning remained constant in these calculations. The red curve with triangles represents the AUH located near the center of the ship, the curve with black squares indicates a position near the rear midship, and the blue curve with dots indicates an AUH located near the stern of the ship.

For surge, shown in Figure 4a, AUH oscillations were significantly higher in Positions 1 and 2 than Position 3. For heave, in Figure 4b, all three curves reached a small peak when wave frequency reached 1 rad/s (indicating the AUH reached its resonance frequency), and Position 2 was unstable at this frequency. In practice, this wave frequency should be avoided. For roll, in Figure 3c it can be seen that the AUH oscillated more intensely than in Position 1. For pitch, in Figure 4d, AUH oscillations were most pronounced in Position 2. The results of the above analysis showed that oscillation amplitude in Position 3 was the smallest, indicating this position could be selected as an appropriate launch or recovery location. Three cases study were conducted to select three different Y_1 position in the same $X_1 - Z_1$ plane, as shown in Table 3.

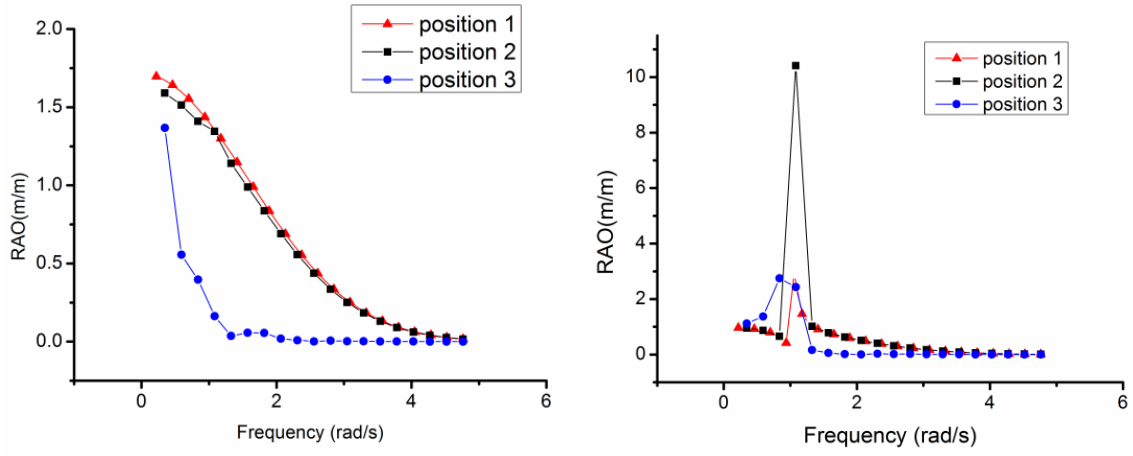

(**a**) (**b**)

Figure 4. *Cont.*

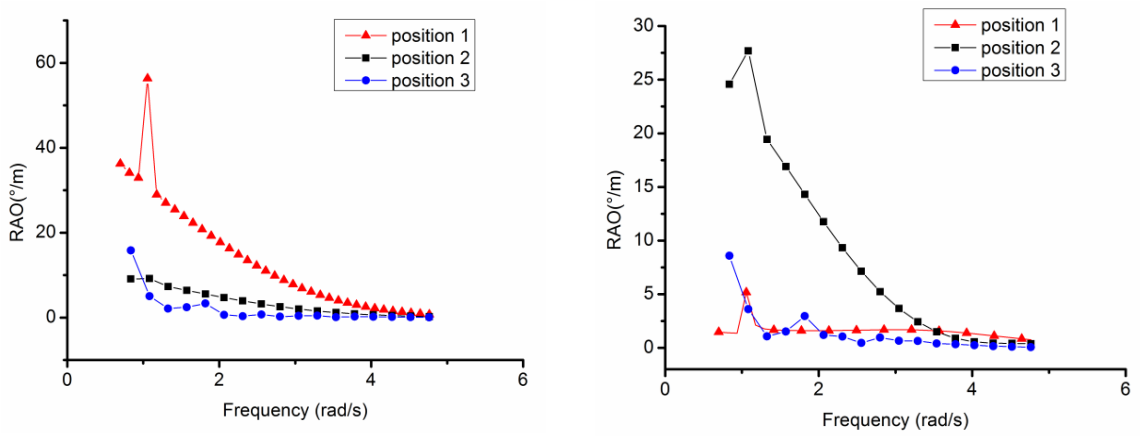

Figure 4. Six-degrees-of-freedom (6-DOF) motion response amplitude operators (RAOs) of AUH located in three different positions in X-axis. (**a**) Surge; (**b**) heave; (**c**) roll; (**d**) pitch.

For surge, as shown in Figure 5a, the AUH oscillates more slowly in Position 2. For heave, shown in Figure 5b, the three curves reach a peak when wave frequency is 1 rad/s (indicating a resonance phenomenon), implying work with AUHs should avoid these conditions. For pitch, seen in Figure 5c, the AUH is unstable at Position 3 with a wave frequency of 1 rad/s. For yaw, seen in Figure 5d, AUH oscillation amplitudes at Positions 1 and 2 are larger than at Position 3. Overall, Position 1 is shown to be the favorable location for AUH recovery and launch.

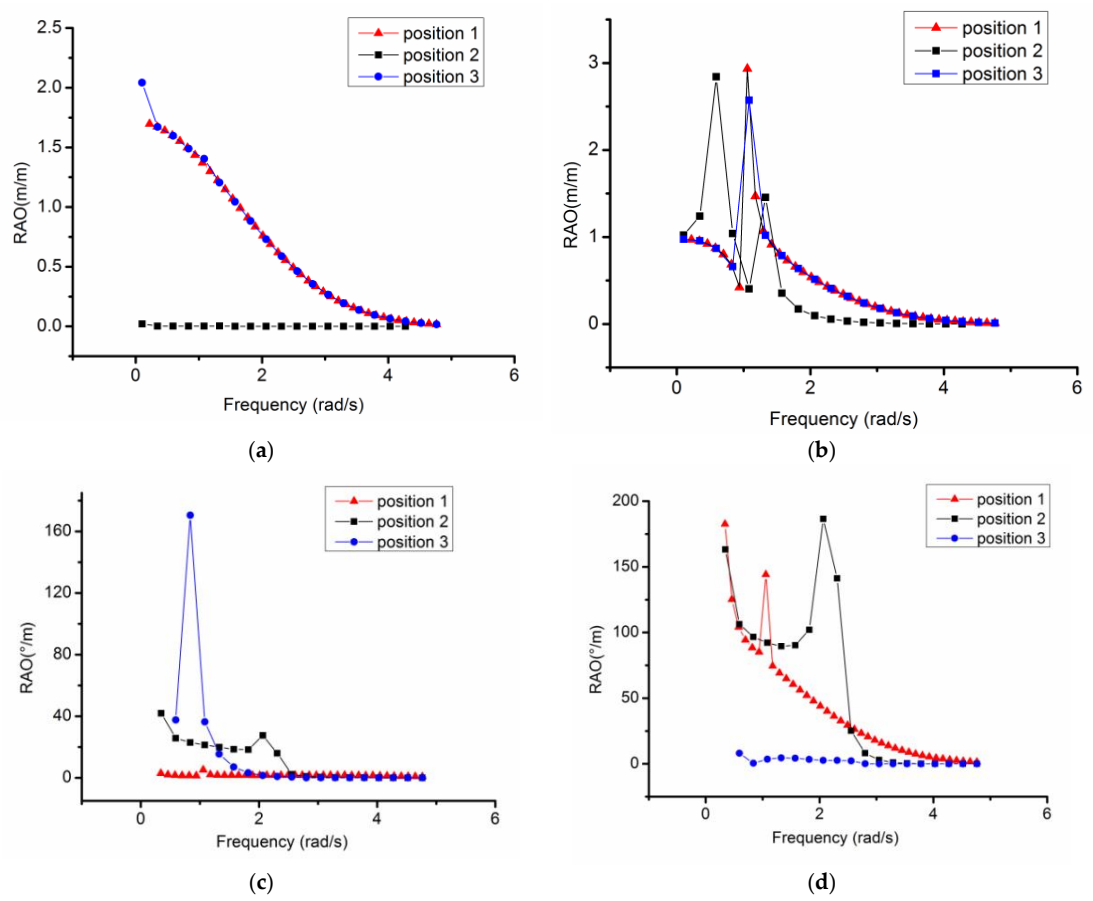

Figure 5. AUH 6-DOF RAOs in different position in Y-axis. (**a**) Surge; (**b**) heave; (**c**) pitch; (**d**) yaw.

3.2. Comparing AUH and AUH–Ship RAOs in Optimal Positions

Position $X_1 = 3$ m, $Y_1 = -2.4$ m, $Z_1 = -2$ m in the host-ship coordinate system was selected as the launch and recovery position due to its smaller oscillation amplitude in the above calculation results, indicating significant workforce and material-resource savings. This study examined the interference of the host ship with the AUH during recovery at the stern of the host ship. Motion RAO variations in the 6-DOF of AUH–Ship interactions are shown in Figure 6a–f for AUHs in the three investigated locations. Figure 6 shows that the host ship exerts significant influence on the AUH RAOs, especially sway and pitch. In sway, as shown in Figure 6b, the presence of the host ship greatly increases AUH oscillations, deteriorating the seakeeping performance of the AUH.

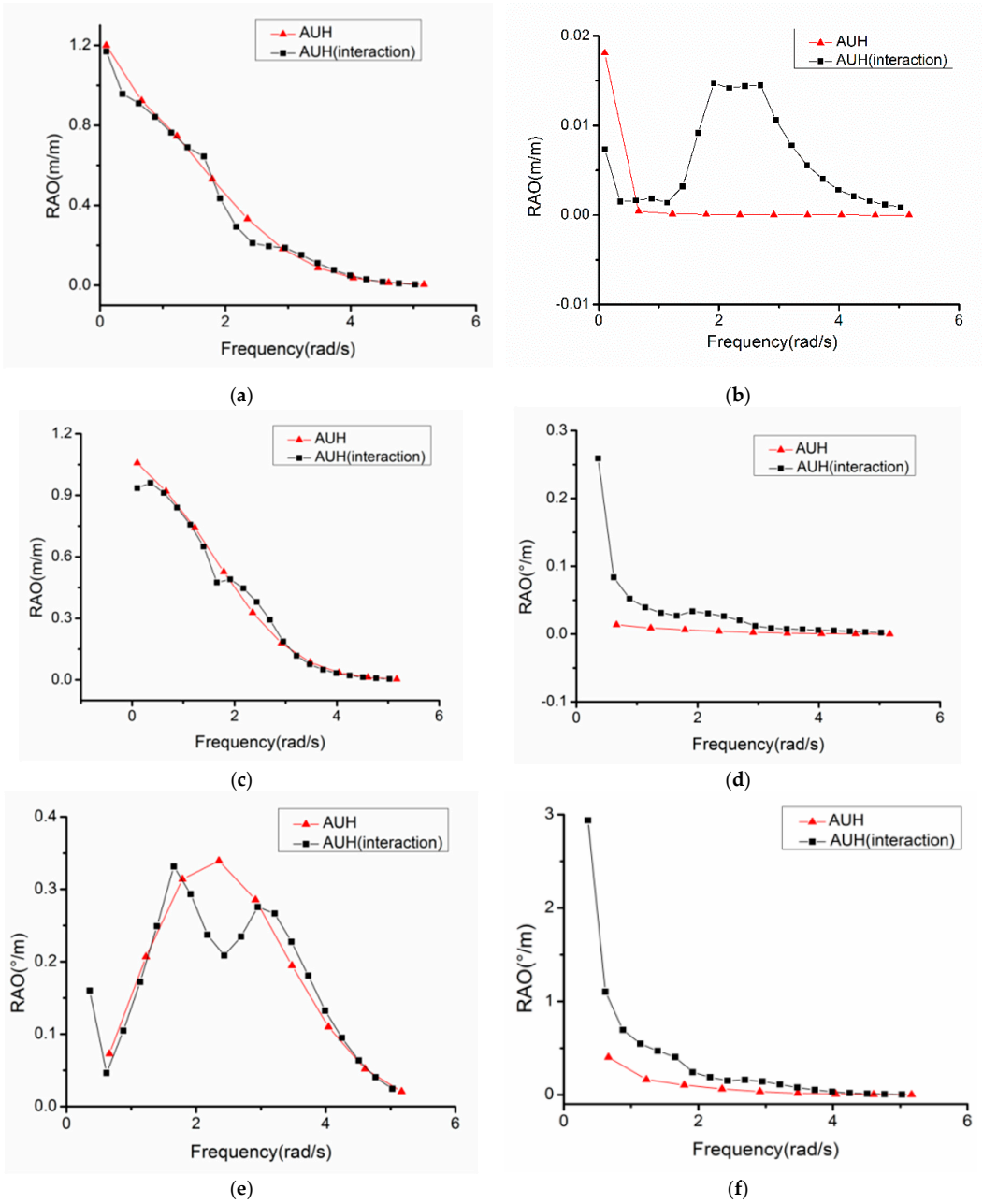

Figure 6. Six-DOF RAOs of AUH in special position. (**a**) Surge; (**b**) sway; (**c**) heave; (**d**) roll; (**e**) pitch; (**f**) yaw.

3.3. Hydrodynamic Interaction at Different Inflow Velocities

The hydrodynamic interaction of the AUH at different inflow velocities was calculated in the same conditions as Section 3.2 to observe their influence. Figure 7 shows the 2-DOF RAOs of the AUH in roll and yaw under different inflow velocities of 0.5–3.0 knots when disturbed by the host ship.

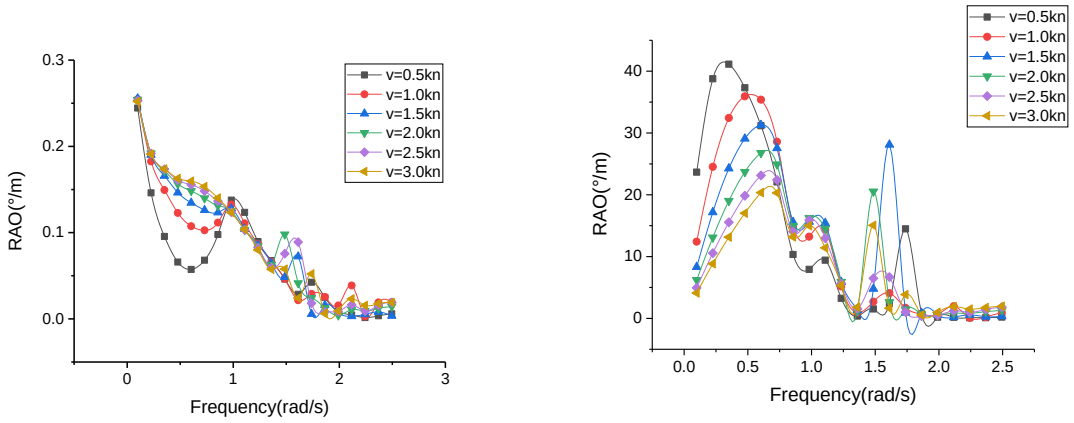

Figure 7. Two-DOF RAOs of AUH in different inflow velocities. (**a**) Roll and (**b**) yaw.

Figure 7 shows that AUH motion responses in roll and yaw are different when the AUH is at different velocities. At low wave frequencies, impact on AUH motion can be experienced. When controlling AUH maneuverability, special attention should be paid to the movement amplitude of the AUH at low frequency in order to prevent it from being in dangerous conditions.

3.4. AUH–Ship Interaction Motion in Irregular Waves

Time-domain analysis for an AUH at a specific location was conducted to further analyze the hydrodynamic interactions of AUHs influenced by disturbances from the host ship in irregular waves. Long-crested irregular waves were superimposed over a number of regular waves of different amplitudes and wavelengths, which could be expressed by a frequency spectrum [32]. According to analysis by Soares [32], wave-load response depends on spectral-model selection, including long- and short-crested irregular sea models. The former model is referred to as fully developed in the dominant wind direction. The latter represents wave crests formed at the right angles to the wind direction with waves propagating in different directions with a dominant spreading direction (directional spectrum). A motion-response spectrum [33] is given by

$$S_r(\omega_E, \chi) = \left|RAO(\omega_E, \chi)\right|^2 S_\zeta(\omega_E, \chi) \tag{11}$$

where $S_\zeta(\omega_E, \chi)$ represents a known seaway spectrum incorporating encounter frequency ω_E and encounter angle χ; $S_r(\omega_E, \chi)$ represents the response spectrum of r in 6-DOF (surge, sway, heave, roll, pitch, and yaw) within the distribution of the amplitude squared over ω_E and χ; elementary-wave-motion RAOs for the response spectrum of r were calculated as in Equation (9).

For long-crested irregular seas, this study adopted the Pierson–Moskowitz (P–M) wave-spectrum model to study AUH–Ship interaction-performance limitations in time series, as this spectrum is sufficient to cover many oceanic observations [34]. In this study, the significant wave height of 1 m of the P–M spectrum was translated into a time series, as shown in Figure 8, for time-variation simulations of RAO-based AUH motion in 6-DOF, as shown in Figure 9. The P–M wave spectrum is expressed as

$$S_X(\omega) = \frac{0.78}{\omega^5} \exp\left\{\frac{-0.78 g_4}{U'\omega_4}\right\} (m^2 s) \tag{12}$$

where U' is wind speed at a height of 19.5 m. This wind speed can be determined using

$$U' = 6.85\sqrt{h_{1/3}} \tag{13}$$

where $h_{1/3}$ is the significant wave height (1 m) and zero crossing period of 10 s. AUH and host-ship speeds are 0 knots for both, the encounter angle is 0° (following sea), and the resonant frequency value is

$$\omega_0 = 0.4\sqrt{g/h_{1/3}} \tag{14}$$

The time series for wave-elevation numerical simulations, as shown in Figure 8, can be generated by Equation (15).

$$\zeta(x, y, t) = \sum_{n=1}^{N} \sqrt{2S_\zeta(\omega^*)\Delta\omega} \cos(\omega^* t + \varepsilon_n - k_n(x\cos\chi - y\sin\chi)) \tag{15}$$

where wave height $\zeta(x, y, t)$ incorporates space and time with ω^* taken randomly in each interval $[\omega_n - \Delta\omega/2, \omega_n + \Delta\omega/2]$ [35].

The 6-DOF RAO–based motion response of the AUH interacting with the ship in a time series with different wave directions is shown in Figures 9a–f and 10a–f, depicting AUH motions in surge (a), sway (b), heave (c), roll (d), pitch (e), and yaw (f). The speed of the AUH and the host ship is 0 knots and the wave-encounter angles are 0° and 90° (following sea and beam sea, respectively). In Figures 9 and 10, the oscillation amplitude of each DOF at different wave angles in irregular waves is not large, and the yaw amplitude, the largest of the DOFs, is up to 1 m. The simulation results of the RAO-based AUH responses show that the AUH moves gently in this position, making it a viable recovery and launch position.

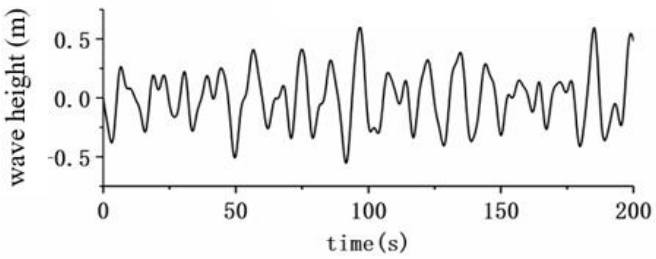

Figure 8. Time series at origin for Pierson–Moskowitz (P–M) spectrum for significant wave height of 1 m.

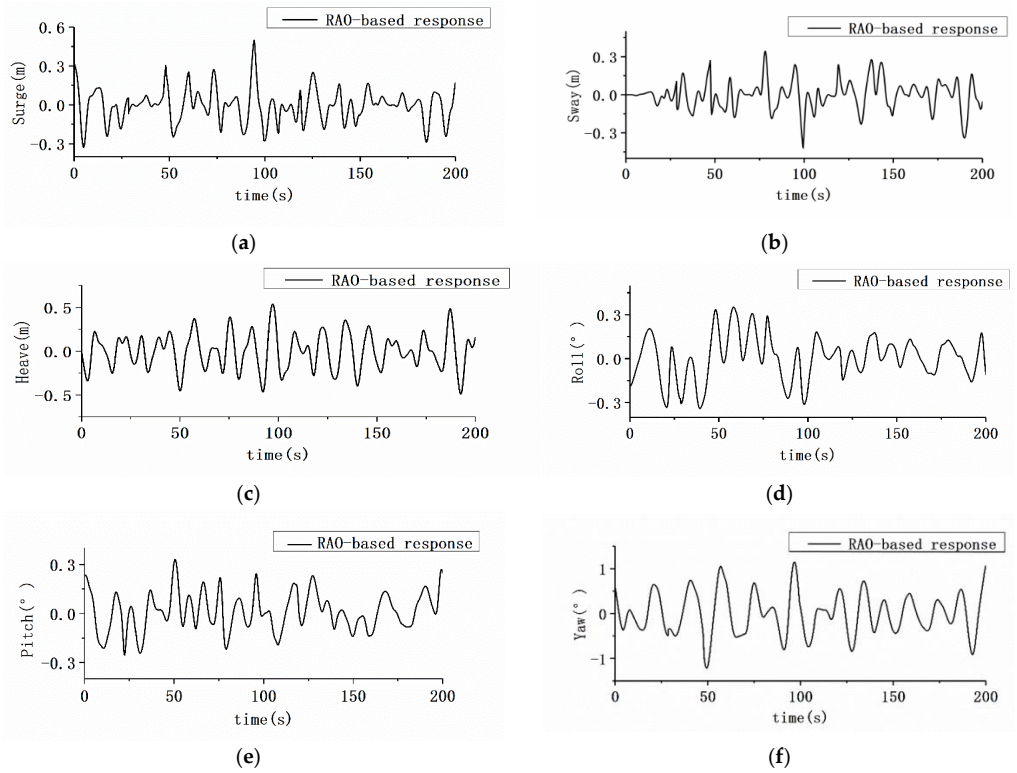

Figure 9. Time-series of RAO-based AUH motion in 6-DOF in following sea. (**a**) Surge; (**b**) sway; (**c**) heave; (**d**) roll; (**e**) pitch; (**f**) yaw.

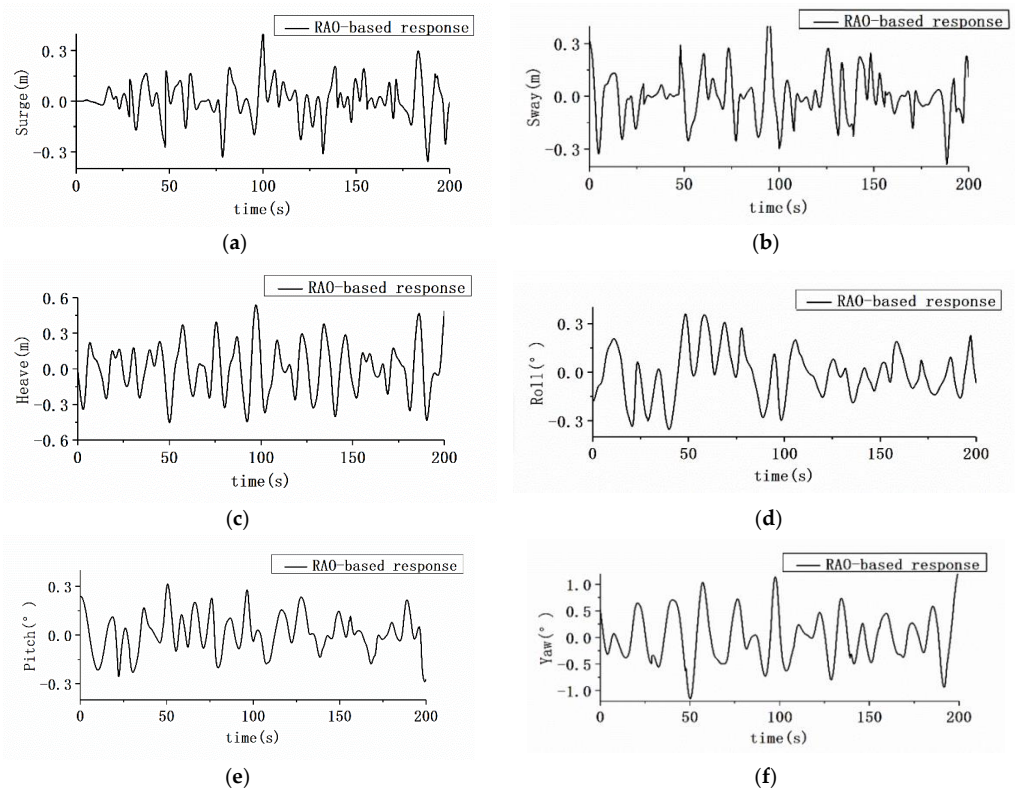

Figure 10. Time-series of RAO-based AUH motion in 6-DOF in beam sea. (**a**) Surge; (**b**) sway; (**c**) heave; (**d**) roll; (**e**) pitch; (**f**) yaw.

4. Experiment Validation

The experiments were carried out in the large-scale cross-sectional wave flume of Zhejiang University Ocean College in Zhoushan in December 2017. The flume was 75 m in length, 2 m in height, and 1.8 m in width, as shown in Figure 11a; the AUH was preadjusted to neutral buoyancy and then placed in the flume. A diagrammatic sketch of the wave-flume cross-section within the AUH is shown in Figure 11b. There was a wave maker at the end of the flume that could generate regular and irregular waves within a 0.5–5.0 s wave-period range and 0.02–0.6 m wave-height range. The waves in frequency range of 0.2–1.0 rad/s were made in the experiment to simulate a moderate sea state for recovering AUH in waves. The perspective view of the wave flume is shown in Figure 11c. The simulations of the wave flume and AUH with discrete panels, boundary conditions, and wave propagation direction for validation study is as shown in Figure 11d.

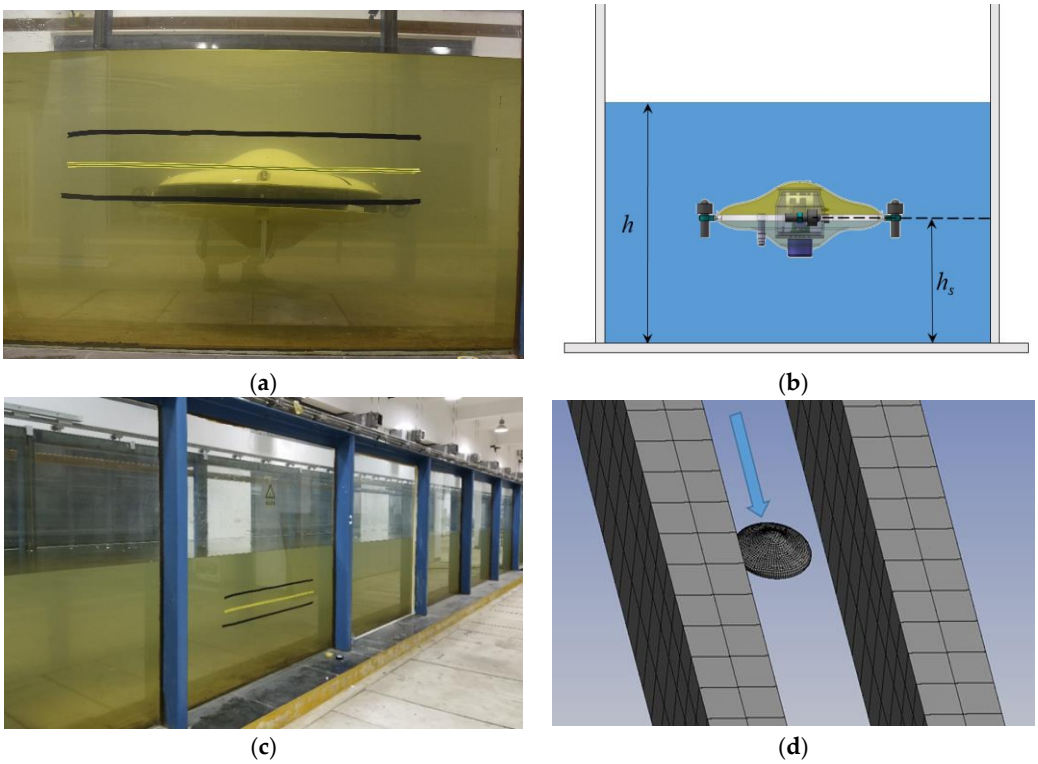

Figure 11. (**a**) AUH set in experiment wave flume in lateral view; (**b**) diagrammatic sketch of AUH in wave flume in frontal view; (**c**) wave flume with total length of 75 m; (**d**) simulation model of the wave flume and AUH.

The purpose of this experiment was to verify the accuracy of the numerical calculation results of the AUH wave force. Water depth h was 1.2 m, and distance h_S from bottom to the center of gravity was 0.6 m. Wave period T_w was set as 1, 1.5, 2, 2.5, 3, 3.5, 4, 4.5, and 5 s, and wave height H_w was set as 0.1 and 0.2 m. A WT901BLE-type attitude sensor was used to record AUH motion angle and angular-velocity information. Sensor measurement stability was 0.05°, and output frequency was 10 Hz.

The rolling angle of the AUH for different wave periods and heights was measured. Figure 12a–c shows the rolling angles of AUH change over time in three conditions: (1) $T_w = 2$s, $H_w = 0.2$m, (2) $T_w = 2.5$s, $H_w = 0.2$m, and (3) $T_w = 5$s, $H_w = 0.1$m. The rolling-angle response was more regular in high-frequency waves when compared to that in low-frequency waves.

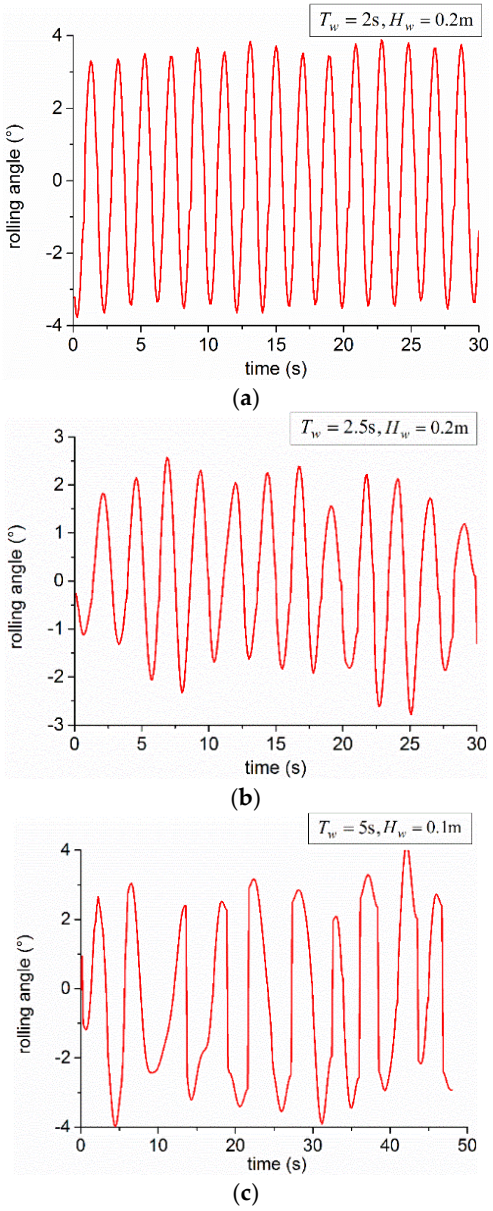

Figure 12. AUH rolling response in regular waves.

At the same time, AUH Numerical Simulation 1 in the restricted flume was conducted as shown in Figure 13. The boundary conditions were set in accordance with the experiment. Due to ANSYS-AQWA being potential-based hydrodynamic-simulation software, damping influence was neglected. Damping has great influence on the rolling motion of the AUH, i.e., viscous damping forces playing an important role while the AUH is in the condition where the lower wave frequency implies the greater wavelength encountered. The factor of damping was taken into account in Numerical Simulation 2, which increased the accuracy of the numerical simulation of the rolling direction. The improved effectiveness is obvious especially at low frequencies, as in Table 4. The proposed damping term for the vertical axisymmetrical AUH can be expressed as

$$D_{critical} = 2\sqrt{mK} = 2\sqrt{(I_{xx} + \Delta I_{xx})K_{Roll}} \quad (16)$$

where $D_{critical}$ represents critical damping; I_{xx} represents rolling inertia mass; K_{Roll} represents rolling stiffness matrix; and K and ΔI_{xx} represent the stiffness of corresponding degrees of freedom and added mass inertia mass, respectively.

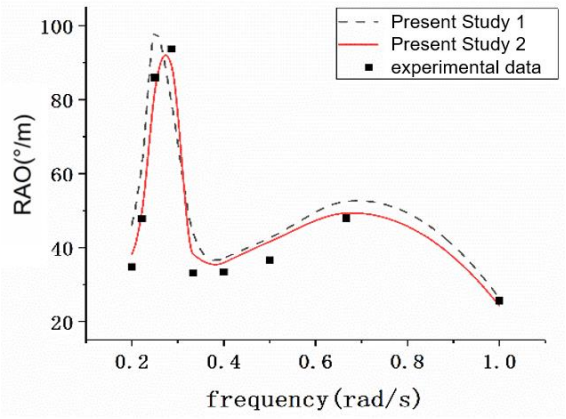

Figure 13. Comparison of RAO variations in roll versus wave frequency using the panel methods and experiment data.

Table 4. Comparison between experiment data and numerical results.

Frequency (Hz)	Experiment Data (°/m)	Study 1 (°/m)	Error 1	Study 2 (°/m)	Error 2
1	32.3	26.3	18.6%	24.3	14.13%
0.67	45.6	52.5	15.1%	49.3	8.11%
0.5	36.8	42.6	15.8%	41.6	13.04%
0.4	34.3	37.1	8.2%	35.9	4.67%
0.33	34.1	44.1	29.3%	38.3	12.32%
0.29	82.2	79.4	3.4%	89.3	9.97%
0.25	75.2	98.2	30.6%	82.3	9.44%
0.22	45.5	62.7	37.8%	49.9	9.67%
0.2	35.4	46.2	30.5%	38.3	8.19%
Average error		21.03%		9.95%	

A comparison between numerical results of the AUH rolling RAO and the experiment data is shown in Figure 13 and Table 4. The overall trend of the AUH motion RAO in rolling was relatively consistent. From Table 4 we know that in wave-frequency range 0.2–1.0 Hz, the average error of the AUH rolling RAO was 21% in different wave frequencies, and minimum error was 3.4% in 2.9 Hz. Within the limits of experimental error and sensor precision, viscous force was not considered in the numerical calculation. Thus, the tolerance error was acceptable to prove the numerical results as a valid and rational. Study 1 was further optimized, and the results of Study 2 were more accurate by adding the damping term, as shown in Equation (16). This process reduced the error from 21.03% to 9.95%.

5. Conclusions

This study analyzed the hydrodynamic interaction of a new type of underwater robot, the AUH, in locations near a host ship using the computational fluid dynamic ANSYS-AQWA solver, a potential–based panel method. The simulation results of the investigated AUH–Ship interactions are significant to practical works, including research on automated ship recovery and launch systems to be used in advance for AUH operations in waves. This research can significantly enhance the efficiency of AUH homing automation to host ships in waves. The 6-DOF RAOs of an AUH at various distances from the host ship were predicted, and a suitable location area for AUH launch and recovery was determined.

The host ship exerted significant influence on AUH motion performance in sway and pitch. The influence of the host ship on interactive AUH hydrodynamic disturbances was determined in terms of 6-DOF RAOs. The RAOs of the AUH at different velocities were successfully predicted for enhanced adaptive controllability of homing automation. A specific location for optimizing AUH seakeeping

performance during recovery and launch operations in long-crested irregular waves was analyzed in the time domain using the P–M wave-spectrum model to observe good positions. Simulation results showed that the sea condition with a wave frequency of 1 rad/s should be avoided due to the resonance phenomenon. AUH oscillation amplitude was the smallest at X = 3 m, Y = −2.4 m, Z = −2 m, and X = 10 m, Y = −2.4 m, Z = −2 m; these positions should be selected as an appropriate location for launch or recovery.

Experiment validation of the dish-type AUH motion RAO during roll and pitch was carried out. Numerical analysis of motion RAO in roll with a proposed damping model was compared to experiment data in the wave-frequency range of 0.2–1.0 Hz, resulting in average errors being reduced from 21.03% to 9.95%, verifying the accuracy of the adopted method. Comparisons between numerical results and experiment data showed that the tolerance error was acceptable to prove that the numerical results were valid and rational. In the future, AUH behavior induced by sensors and controllability in short-crested irregular waves will be further studied. An experimental study of the designed AUH configurations mounted with different aquatic transducer lengths, to achieve an acceptable trade-off between hydrodynamic optimization and acoustic navigation, will be carried out in future research and for practical applications.

Author Contributions: Conceptualization, C.-W.C.; Data curation, Y.C.; Formal analysis, C.-W.C. and Q.-W.C.; Funding acquisition, C.-W.C. and Y.C.; Investigation, C.-W.C. and Y.C.; Methodology, C.-W.C., Y.C. and Q.-W.C.; Project administration, Y.C.; Resources, Q.-W.C.; Software, C.-W.C., Y.C. and Q.-W.C.; Visualization, C.-W.C., Y.C. and Q.-W.C.; Writing—original draft, C.-W.C. and Q.-W.C.

Acknowledgments: The authors wish to thank the National Key Research and Development Program of China (No. 2017YFC0306100), and the National Natural Science Foundation of China (No. 51409230) for financially supporting the research on the hydrodynamic behavior of the Autonomous Underwater Hovering Vehicle.

Conflicts of Interest: The authors declare no conflict of interest.

Nomenclature

\	**Velocity potential**
U	AUH speed
–Ux	AUH sailing at a constant speed U
ϕ	Perturbation potential induced byAUH presence
S_B	Body boundary
$\mathbf{U} \cdot \mathbf{n}$	Normal velocity on the AUH boundary
S_H	Sea-bottom boundary
ω_E	Wave-encounter frequency
ϕ_{I}	Velocity potential of incident wave
ϕ_{D}	Diffraction power of multifloating system
ϕ_{R1}	Radiation potential of floating body 1 in multifloating system
ϕ_{R2}	Radiation potential of floating body 2 in multifloating system
Re{}	Real part of amount in {}
H_w	Wave height
$X_2Y_2Z_2$	Position of AUH in body-fixed coordinates
h_S	Distance from bottom to center of gravity
CG, CB	Center of gravity, center of buoyancy
AUH	Autonomous Underwater Helicopter
AUH–Ship	Study on hydrodynamic interaction between AUH and Ship
ζ	**Wave height**
ξ	Bottom clearance coefficient
T	AUH height
RAO	Response amplitude operator
χ	Wave encounter angle
S_ζ	Seaway spectrum

S_r	Response spectrum of r in 6-DOF of surge, sway, heave, roll, pitch, and yaw
U′	Wind speed at height of 19.5 m
η_i	Magnitude of i-DOF of floating body
t	Nearest vertical distance between AUH and slope
T_w	Wave period
$D_{critical}$	Critical damping
I_{xx}	Rolling inertia mass
K_{Roll}	Rolling stiffness matrix
K	Stiffness of corresponding degrees of freedom
ΔI_{xx}	Added mass inertia mass
BG	Vertical distance between the CB and CG
RAO	Response Amplitude Operator

References

1. Ribas, D.; Palomeras, N.; Ridao, P.; Carreras, M.; Mallios, A. Girona 500 AUV: From Survey to Intervention. *IEEE/ASME Trans. Mechatron.* **2012**, *17*, 46–53. [CrossRef]
2. Yang, R.; Clement, B.; Mansour, A.; Li, M.; Wu, N. Modeling of a Complex-Shaped Underwater Vehicle for Robust Control Scheme. *J. Intell. Robot. Syst.* **2015**, *80*, 491–506. [CrossRef]
3. Chen, Q.; Su, R. Analysis of launch and recovery UUV model for submarine. *Ship Sci. Technol.* **2011**, *33*, 146–149.
4. Sarda, E.I.; Dhanak, M.R. A USV-Based Automated Launch and Recovery System for AUVs. *IEEE J. Ocean. Eng.* **2017**, *42*, 37–55. [CrossRef]
5. Wu, L.; Li, Y.; Su, S.; Yan, P.; Qin, Y. Hydrodynamic Analysis of AUV Underwater Docking with a Cone-Shaped Dock under Ocean Currents. *Ocean Eng.* **2014**, *85*, 110–112. [CrossRef]
6. Xie, N.; Iglesias, G.; Hann, M.; Pemberton, R.; Greaves, D. Experimental Study of Wave Loads on a Small Vehicle in Close Proximity to a Large Vessel. *Appl. Ocean Res.* **2019**, *83*, 77–87. [CrossRef]
7. Skomal, G.B.; Hoyos-Padilla, E.M.; Kukulya, A.; Stokey, R. Subsurface Observations of White Shark Carcharodon Carcharias Predatory Behaviour using an Autonomous Underwater Vehicle. *J. Fish Biol.* **2015**, *87*, 1293–1312. [CrossRef]
8. Leong, Z.Q.; Ranmuthugala, D.; Penesis, I.; Nguyen, H. Quasi-Static Analysis of the Hydrodynamic Interaction Effects on an Autonomous Underwater Vehicle Operating in Proximity to a Moving Submarine. *Ocean Eng.* **2015**, *106*, 175–188. [CrossRef]
9. Tian, W.; Song, B.; Ding, H. Numerical Research on the Influence of Surface Waves on the Hydrodynamic Performance of an AUV. *Ocean Eng.* **2019**, *183*, 40–56. [CrossRef]
10. Mansoorzadeh, S.; Javanmard, E. An Investigation of Free Surface Effects on Drag and Lift Coefficients of an Autonomous Underwater Vehicle (AUV) using Computational and Experimental Fluid Dynamics Methods. *J. Fluids Struct.* **2014**, *51*, 161–171. [CrossRef]
11. Malik, S.A.; Pan, G.; Liu, Y. Numerical Simulations for the Prediction of Wave Forces on Underwater Vehicle using 3D Panel Method Code. *Res. J. Appl. Sci. Eng. Technol.* **2013**, *5*, 5012–5021. [CrossRef]
12. Lighthill, M.J. Waves and hydrodynamic loading. In Proceedings of the Second International Conference on the Behaviour of Offshore Structures, London, UK, 7–10 July 1979.
13. Chen, G.-R.; Fang, M.-C. Hydrodynamic interactions between two ships advancing in waves. *Ocean Eng.* **2001**, *28*, 1053–1078. [CrossRef]
14. Choi, Y.R.; Hong, S.Y. An analysis of Hydrodynamic Interaction of Floating Multi-body Using High-Order Boundary Element Method. In Proceedings of the Twelfth International Offshore and Polar Engineering Conference, Kitakyushu, Japan, 26–31 May 2002; pp. 303–308.
15. Masashi, K.; Kazuaki, E.; Hiroshi, Y. Wave Drift Force and Moments on Two Ships Arranged side by side in Waves. *Ocean Eng.* **2005**, *32*, 529–555.
16. Hong, S.Y.; Kim, J.H.; Cho, S.K.; Choi, Y.R.; Kim, Y.S. Numerical and Experimental study on Hydrodynamic Interaction of side-by-side moored Multiple Vessels. *Ocean Eng.* **2005**, *32*, 783–801. [CrossRef]
17. Chen, C.W.; Jiang, Y.; Huang, C.H.; Ji, D.X.; Sun, G.Q.; Yu, Z.; Chen, Y. Computational fluid dynamics study of the motion stability of an autonomous underwater helicopter. *Ocean Eng.* **2017**, *143*, 227–239. [CrossRef]

18. Chen, C.W.; Huang, C.H.; Dai, X.K.; Huang, H.C.; Chen, Y. Motion and Control Simulation of a Dished Autonomous Underwater Helicopter. In Proceedings of the OCEANS 2017, Anchorage, AK, USA, 18–21 September 2017; pp. 1–6.
19. Chen, C.W.; Yan, N.M.; Leng, J.X.; Chen, Y. Numerical Analysis of Second-Order Wave Forces Acting on an Autonomous Underwater Helicopter using Panel Method. In Proceedings of the OCEANS 2017, Anchorage, AK, USA, 18–21 September 2017.
20. Chen, C.-W.; Jiang, Y. Computational Fluid Dynamics Study of Magnus Force on an Axis-Symmetric, Disk-Type AUV with Symmetric Propulsion. *Symmetry* **2019**, *11*, 397. [CrossRef]
21. Chen, C.W.; Yan, N.M. Prediction of Added Mass for an Autonomous Underwater Vehicle Moving Near Sea Bottom Using Panel Method. In Proceedings of the 2017 4th International Conference on Information Science and Control Engineering (ICISCE), Changsha, China, 21–23 July 2017; pp. 1094–1098.
22. Miller, P.A.; Farrell, J.A.; Zhao, Y.; Djapic, V. Autonomous Underwater Vehicle Navigation. *IEEE J. Ocean. Eng.* **2010**, *35*, 663–678. [CrossRef]
23. He, B.; Zhang, H.; Li, C.; Zhang, S.; Liang, Y.; Yan, T. Autonomous Navigation for Autonomous Underwater Vehicles Based on Information Filters and Active Sensing. *Sensors* **2011**, *11*, 10958–10980. [CrossRef]
24. Pérez-Alcocer, R.; Torres-Méndez, L.A.; Olguín-Díaz, E.; Maldonado-Ramírez, A.A. Vision-Based Autonomous Underwater Vehicle Navigation in Poor Visibility Conditions using a Model-Free Robust Control. *J. Sens.* **2016**, *2016*, 1–16. [CrossRef]
25. Ji, D.; Li, H.; Chen, C.W.; Song, W.; Zhu, S. Visual Detection and Feature Recognition of Underwater Target using a Novel Model-Based Method. *Int. J. Adv. Robot. Syst.* **2018**, *15*. [CrossRef]
26. Rauch, C.G.; Purcell, M.J.; Austin, T.; Packard, G.J. Ship of opportunity launch and recovery system for REMUS 600 AUV's. In Proceedings of the OCEANS 2008, Quebec City, QC, Canada, 15–18 September 2008.
27. Sharp, K.; Cronin, D.; Small, D.; Swanson, R.; Augustus, T. A cocoon-based shipboard launch and recovery system for large autonomous underwater vehicles. In Proceedings of the MTS/IEEE Oceans 2001, Honolulu, HI, USA, 5–8 November 2001.
28. Newman, J.N.; Landweber, L. Marine Hydrodynamics. *J. Appl. Mech.* **1977**, *45*, 457. [CrossRef]
29. Joseph, D.D. Potential flow of viscous fluids: Historical notes. *Int. J. Multiph. Flow* **2005**, *32*, 285–310. [CrossRef]
30. Seif, M.S.; Inoue, Y. Dynamic analysis of floating bridges. *Mar. Struct.* **1998**, *11*, 29–46. [CrossRef]
31. Sun, B.; Miao, Q.; Feng, X.; Jiang, H. A Numerical Method for the Calculation of the Wave Forces Acting on a Submarine Travelling near the Free Surface. *J. Ship Mech.* **1997**, *1*, 21–26.
32. Soares, C.G. Effect of spectral shape uncertainty in the short term wave-induced ship response. *Appl. Ocean Res.* **1990**, *12*, 54–69. [CrossRef]
33. Perez, T. *Ship Motion Control: Course Keeping and Roll Stabilisation Using Rudder and Fins*; Springer: London, UK, 2005.
34. Moreira, L.; Soares, C.G. H_2 and H_∞ Designs for Diving and Course Control of an Autonomous Underwater Vehicle in Presence of Waves. *IEEE J. Ocean. Eng.* **2008**, *33*, 69–88. [CrossRef]
35. Refsnes, J.E.; Sorensen, A.J.; Pettersen, K.Y. Model-Based Output Feedback Control of Slender-Body Underactuated AUVs: Theory and Experiments. *IEEE Trans. Control Syst. Technol.* **2008**, *16*, 930–946. [CrossRef]